Pergamon

Int. J. Heat Mass Transfer. Vol. 40, No. 10, pp. 2351–2361, 1997

0017–9310/97 $17.00+0.00

PII: S0017–9310(96)00299–2

An experimental study of the heat transfer between near-fluidized particles and an oscillating immersed surface

C. DU and R. TURTON†

Department of Chemical Engineering, West Virginia University, Morgantown, WV 26506, U.S.A.

(*Received* 11 *September* 1995 *and in final form* 16 *August* 1996)

Abstract—A novel heat transfer probe was developed to evaluate heat transfer coefficients between near-fluidized particles and a vibrating heat transfer surface. The periodic motion of the surface caused fluctuations in the instantaneous heat transfer coefficient, h. The parameter affecting the fluctuating amplitude of h was the vibration amplitude of the surface (0.2 and 0.5 mm). The frequency of the applied motion (0, 2, 6 and 10 Hz) affected the frequency of h. At higher frequencies h varied at the applied frequency. However, at the lowest oscillation frequency, 2 Hz, h varied at approximately twice the applied frequency.

1. INTRODUCTION

The heat transfer from a fluidized bed, comprising solids and gas, to an immersed surface or vessel wall is strongly influenced by the local hydrodynamics. Dense beds operate in the bubbling, slugging and turbulent regimes, Kunii and Levenspiel [1], Grace [2]. These beds may be considered to consist of two phases. One phase, the emulsion phase, consists of a mixture of gas and quiescently fluidized solids. The other phase, bubble or lean phase, consists primarily of gas with a few dispersed solids. This two-phase theory of fluidization was originally proposed by Toomey and Johnstone [3] who considered the emulsion phase to consist of solids and gas at minimum fluidizing conditions with all excess gas passing through the bed as particle free bubbles or voids. Although significant deviations from this theory have been observed, Kunii and Levenspiel [1], especially for large particles, Hilligardt and Werther [4], the two-phase theory of fluidization still gives an essentially correct picture of bubbling and slugging beds.

As far as the heat transfer from bubbling beds to immersed surfaces is concerned, the movement of bubbles or voids is the primary reason for the high observed rates of heat transfer. As the bubbles move upward through the bed, they drag solids upward in their wakes thus causing the emulsion phase to circulate within the fluidized bed column, Rowe and Partridge [5]. At any given time, a surface within the bed may be in contact with either a bubble or the emulsion phase. This surface will be exposed to a continually changing bed environment consisting of bubbles and emulsion phase and this transient behavior gives rise to high rates of heat transfer.

In addition to the large-scale motions of bubbles and emulsion phase described above, there is also a small-scale motion in a fluidized bed column. This motion is substantiated by the following facts: (1) particles move relative to each other within the emulsion phase due to the interstitial gas flow within the emulsion, Massimilla and Westwater [6], Decker [7], (2) gas circulates through the bubbles, Davidson and Harrison [8], and (3) the fluidized bed column and any immersed surface, most commonly heat exchange tubes, vibrate during operation. Thus, a specific surface within the fluidized bed column will not only contact various pieces of emulsion and bubbles at different times, but will also be exposed to the small-scale perturbations of the individual particles.

The overall rate of heat transfer from a bed to a surface can be considered to be the sum of three terms. Namely, particle/emulsion phase conduction and convection, gas convection and radiation. For small particle beds at moderate temperatures the dominant mechanism is that of emulsion phase conduction and convection. The effects of hydrodynamics, specifically, large- and small-scale motions of particles, on the emulsion phase conduction and convection terms have been described previously by Du and Turton, [9]. Thus, large-scale motion controls the residence time of the emulsion phase near a heat transfer surface, and thereby affects the heat transfer rate between the emulsion and surface. On the other hand, the small-scale motion mainly affects the voidage of the emulsion phase and the contact between the particles and heat transfer surface, these factors are important for heat transfer at short residence times.

One of the most successful models for fluidized bed heat transfer, using the phenomenological picture

† Author to whom correspondence should be addressed.

NOMENCLATURE

A	heat transfer area, area of tin foil exposed to bed [m^2]
C_p	specific heat capacity [J kg^{-1} °C^{-1}]
d_p	particle diameter [m]
f	frequency [Hz]
h	instantaneous heat transfer coefficient [W m^{-2} K^{-1}]
I	current [A]
k	thermal conductivity [W m^{-1} K^{-1}]
K	coefficient of gas mixing used in equation (12)
p	power into tin foil [W]
q	rate of heat dissipation [W]
Q	heat dissipated to a medium from a probe [J]
R	instantaneous ohmic resistance of tin foil [W]
R_p	particle radius [m]
T	temperature of heat transfer surface [°C]
t	time, or residence time of emulsion [s]
u	air velocity [m s^{-1}]
y	thickness of gas film between a surface and a particle [m]
z	thickness of the tin foil used in the heat probe [m].

Greek symbols

Λ	molecular mean free path [m]
α	thermal diffusivity [m^2 s^{-1}]
β	temperature coefficient of resistance [°C^{-1}]
γ	thermal accommodation coefficient
δ	distance or amplitude of vibration [m]
ε	bed voidage
μ	viscosity of fluidizing medium [kg m^{-1} s^{-1}]
ξ	integration argument [s]
ρ	density [kg m^{-3}]
σ	$2\Lambda(2-\gamma)/\gamma$
τ	residence or response time [s]
ω	phase lag [rad].

Subscripts

bed	fluidized bed
c	critical value
d	due to lag
e	in bulk emulsion
ew	first layer of emulsion next to a immersed surface
g	gas
in	refers to actual or true value
max	maximum
mf	at minimum fluidizing conditions
0	reference or ambient conditions, or superficial
out	refers to value measured and given by heat transfer probe
p	particle
r	response
s	solid
sub	substrate
tin	tin foil
vib	vibration
w	at wall.

Superscript

$\bar{}$	time averaged value.

described above, was developed by Mickley and Fairbanks [10]. This model was based on a penetration type phenomenon whereby packets of fresh emulsion come in contact with the heat transfer surface for a period of time and then are replaced by fresh emulsion packets. This model gives excellent agreement with experimental data for contact times of approximately 1 s and greater, but over-predicts the heat transfer coefficient for shorter contact times, with an infinite value predicted as the contact time goes to zero. The reason for the failure of the Mickley and Fairbanks's model at short contact times is due to the assumption of a homogeneous emulsion phase, which becomes invalid when heat penetrates to only a few layers of particles. There have been basically two approaches to deal with this anomaly. The first is to modify the Mickley and Fairbanks's model either by proposing a contact resistance between emulsion phase and heating surface, Baskakov [11], or by taking the effect of the local high void fraction near the heating surface, which acts as an additional heat transfer resistance, Kubie and Broughton [12], Chandran and Chen [13]. Although good agreement between the experimental data and the modified models has been obtained, the *a priori* prediction of this additional resistance is very difficult for anything but mono-sized spherical particles.

The second approach is to take individual particles near the heating surface as the unit element in the heat transfer analysis. Ernst [14, 15] considered the heat conduction through a gas film of thickness y trapped between a particle and heat transfer surface, and obtained an expression for the limiting heat transfer coefficient as follows:

$$h_{max} = 2\frac{k_g}{R_p}\left[\left(\frac{y}{R_p}+1\right)\ln\left(\frac{R_p}{y}+1\right)-1\right]. \quad (1)$$

This formula correctly predicts that the limiting heat transfer coefficient is a function of interstitial gas ther-

mal conductivity and particle size. With the gas film thickness as a fitting parameter, good correlation between theory and experimental data has been obtained. However, the gas film assumption is difficult to justify from a physical standpoint and is not well accepted. Botterill and Williams [16] and Botterill and Hampshire [17] considered a similar case to Ernst's, but assumed the particles to have a finite heat capacity, which makes the heat transfer analysis complicated, and requires a numerical solution. In order to obtain good agreement between theory and experimental data, for short contact times, these workers had to assume the existence of an additional resistance equivalent to a gas film of the order of one tenth the diameter of the particles.

In yet another approach, Schlünder [18] took a microscopic look at the heat transfer process between a particle and heating surface. He assumed that particles were in point contact with the surface, and argued that at very short contact times heat transfer is limited to the small contact region, where the interstitial gas can not be considered to be a continuum, the so called Smoluchowski effect, Muchowski [19]. His expression for the limiting heat transfer coefficient is:

$$h_{\max} = 2\frac{k_g}{R_p}\left[\left(\frac{\sigma}{R_p}+1\right)\ln\left(\frac{R_p}{\sigma}+1\right)-1\right]. \quad (2)$$

It is interesting to note that equation (2) has the same form as equation (1). Experiments in a stirred bed, Wunschmann and Schlünder [20], indicated that there was good agreement between the theoretical prediction of this model and experimental data for glass beads, but poor agreement for zinc and copper particles.

Decker and Glicksman [21] also took a close look at the contact region between a particle and heating surface. They assumed that due to asperities on the surface of a particle there are many points of contact with the heating surface, and that gas packets trapped between the contacting points act as an additional heat transfer resistance. Their analysis is valid only for residence times greater than about 10 ms, and predicts an infinitely large value of h as residence time approaches zero. Qualitative agreement between theoretical predictions and experimental data using beds at minimum fluidizing conditions was achieved, Gloski *et al.* [22], for low non-zero contact times.

In review of the previous work, all researchers who model the limiting heat transfer coefficient concluded that the heat transfer mechanism at short contact times is governed by the heat conduction through the interstitial gas trapped between a particle and the heating surface. However, all of them assumed that a particle and heating surface are stationary during the entire heat transfer process. In order to insure finite values of the limiting heat transfer coefficient, a fictitious gas film or microscopic properties of the system under consideration must be known in order to predict the finite value of h.

Recently, Du and Turton [9] developed a new model for the limiting heat transfer coefficient. This model assumes that emulsion phase particles which contact a heat transfer surface are not stationary but rather undergo small-scale oscillatory motion. A parametric study of this model indicates that the local relative motion of fluidized particles and a heating surface is an additional important factor affecting the limiting heat transfer coefficient, and that by comparison Schlünder's [18] and Decker and Glicksman's [21] microscopic considerations are of secondary importance. However, a systematic experimental study to address the importance of small-scale relative motion between the heat transfer surface and a fluidized bed is still lacking. The object of this paper is to show how small-scale vibration affects the heat transfer between an immersed surface and a bed of particles for short residence times.

2. DESCRIPTION OF EXPERIMENTAL APPARATUS

The objective of this experimental program was to study the effect of particle–surface relative motion on the heat transfer process, for the residence time range of 50–3000 ms. The apparatus needed to conduct the experimental program consisted of two separate systems and is shown in Fig. 1. The first system was composed of a controller and electromagnets which caused a side-ways vibrating motion of a metal bar immersed in a fluidized bed. Both the frequency and amplitude of the vibrating motion of this bar could be controlled over the ranges of 0–10 Hz and 0–1 mm, respectively. The second system included the electronic circuitry and heat transfer surface necessary to evaluate the transient heat transfer process occurring between the surface, attached to the vibration bar, and the fluidized bed. Detailed descriptions of these two systems are given by Du [23], a brief description of each is also given below.

2.1. *Vibrating bar and control circuitry*

The vibration frequencies and amplitudes of interest were in the ranges of 0–10 Hz and 0–1 mm, respectively. The vibrating bar consisted of a square aluminum rod, 6.25 mm × 6.25 mm, which was held horizontal and allowed to oscillate horizontally and perpendicular to its length, by the use of two supporting rods, at either end. The bar passed through the sides of a 200 mm × 200 mm square bed and was sealed at either end with a pair of rubber bellows, which allowed the bar to move freely back and forth but prevented the loss of bed material, as shown in Fig. 2. These rubber bellows also acted to dampen any induced vibration in the fluidized bed caused by the imposed motion of the bar. At both ends of the bar were located permanent magnets which were positioned inside the electromagnets. Thus by changing the polarity of the electromagnets from N→S→N→,

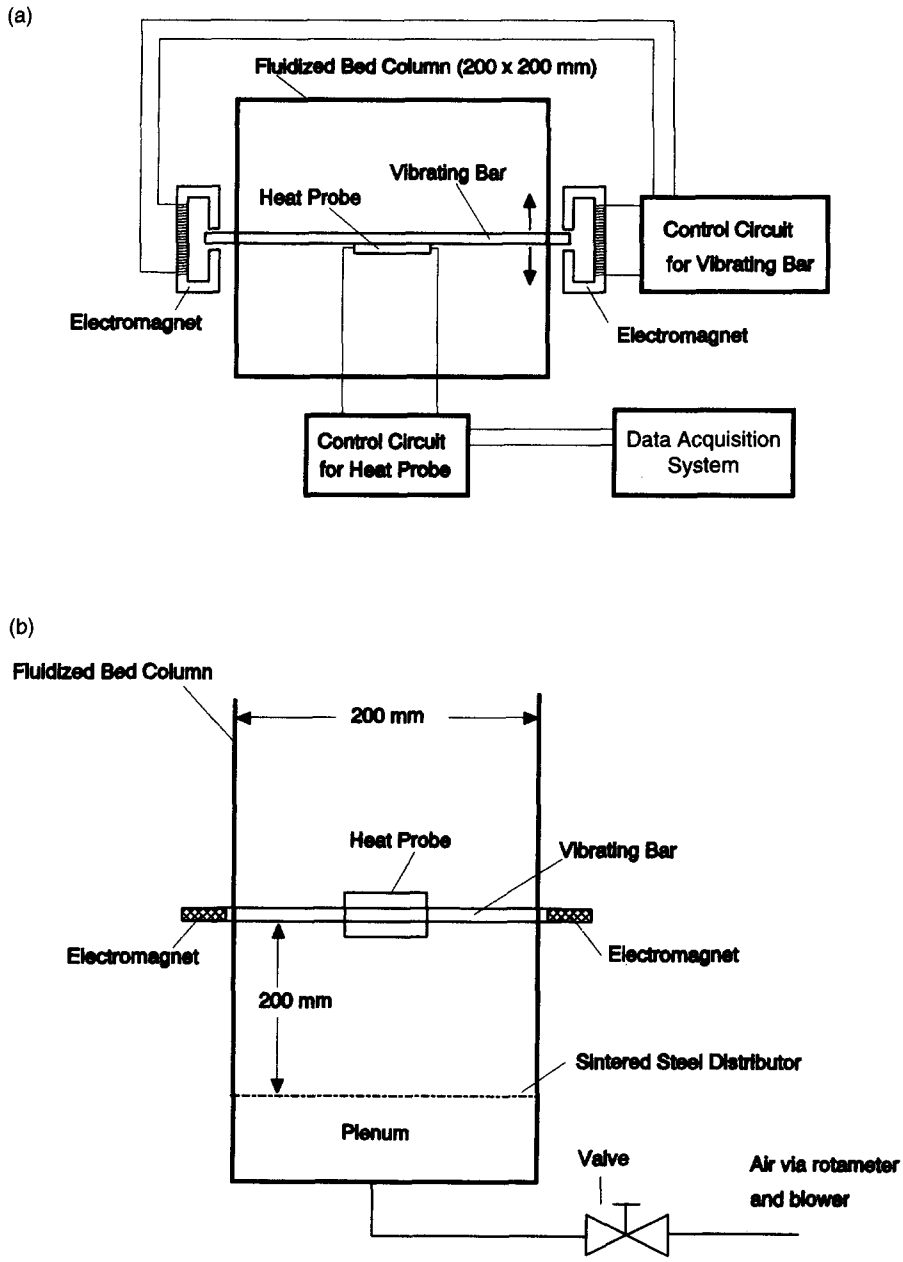

Fig. 1. Schematic diagram of experimental setup.

the bar oscillated back and forth, in a square wave pattern, at the frequency of the changing polarity.

The driver circuit for energizing the electromagnet consisted of a timer, hex invertor, half-H driver, relay, and d.c. power supply. The timer and hex invertor were used to provide a ± 5 mA signal to the half-H driver. This circuit amplified the signal enough to actuate the relay which in turn allowed the d.c. power supply to send a ± 1 A square wave signal to the electromagnets. The frequency of the square wave was controlled by the timer circuit. The distance that the bar could move back and forth was regulated by adjusting set screws at both ends of the bar.

2.2. *Heat transfer probe and control circuitry*

The heat transfer probe is illustrated in Fig. 3. The probe consisted of an expanded polystyrene substrate with a layer of 25 μm thick tin foil which was powered by the probe control circuitry. The pattern of the heat probe, shown in Fig. 3, was obtained by chemically etching the tin foil and then gluing it to the substrate. The heating element had a resistance of approximately 5 W.

The control circuitry used to power the tin foil heating element was capable of providing a high initial current, required to heat the probe to a temperature of 60°C in approximately 20 ms, and then a lower

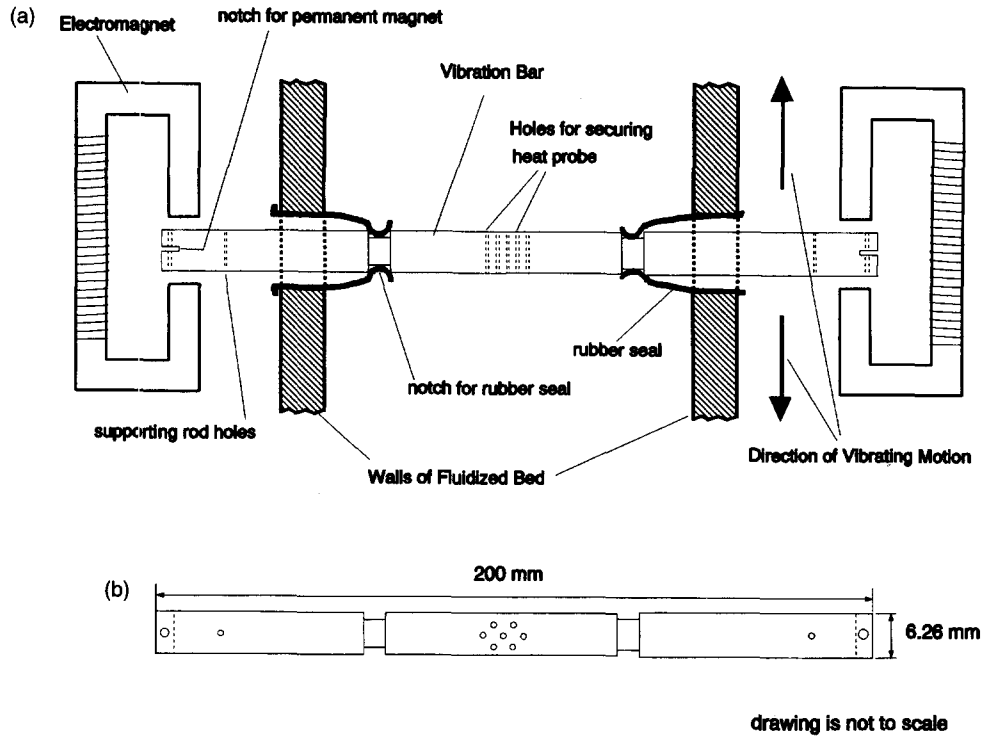

Fig. 2. Diagram of vibration device.

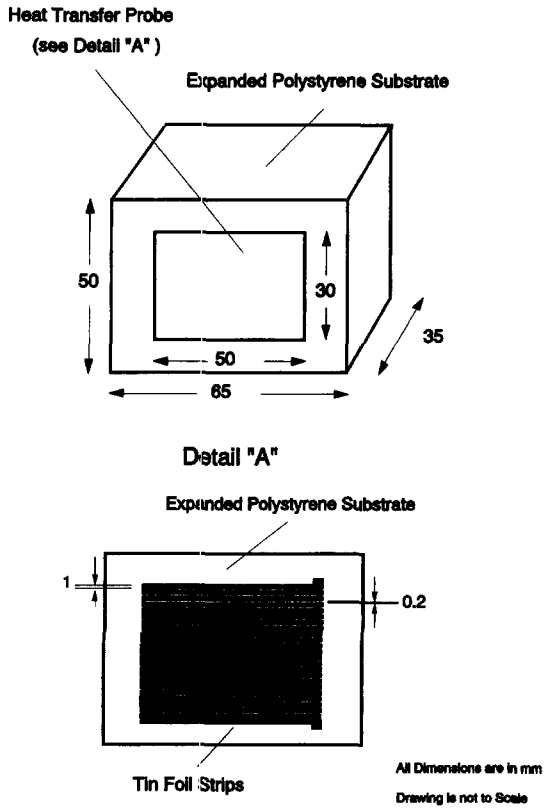

Fig. 3. Diagram of a heat probe.

control current to maintain a constant temperature. The details of the control circuit are given by Du [23]. The values of voltage (V) and current (I) supplied to the heating element were measured and these data were collected by an A/D PC based data acquisition system. From this data the rate of power dissipation from the probe was evaluated.

3. CALIBRATION OF PROBE

The probe was calibrated in both air and ethanol. These two media have thermal properties which bracket those of the fluidized particles used in this work. The calibration was based on a transient energy balance on the heating element of the probe. The calibration experiment involved exposing the probe to air or ethanol and measuring the resistance of the probe and current supplied to the probe with time. The energy input and energy accumulation in the probe were obtained by using the measured resistance and current. The energy output consists of two terms: conduction to the air or ethanol and conduction through the substrate of expanded polystyrene. The first term, i.e. heat transferred to the fluid medium, was calculated by using the well known thermal properties of air and ethanol. Since the calibration was carried out over a very short time period the effects of natural convection could be safely ignored

Table 1. Thermal properties of tin foil and substrate

Material	Thermal property	Value
Tin	Density, ρ	7290 [kg m^{-3}]
	Thermal diffusivity, α	4.30×10^{-5} [m^2 s^{-1}]
	Thermal conductivity, k	68.20 [W m^{-1} K^{-1}]
	Specific heat capacity, C_p	222 [J kg^{-1} K^{-1}]
	Temperature coefficient of resistance, β	4.70×10^{-3} [°C^{-1}]
Substrate (expanded polystyrene)	Density, ρ	40.0 [kg m^{-3}]
	Thermal diffusivity, α	7.60×10^{-7} [m^2 s^{-1}]
	Thermal conductivity, k	3.50×10^{-2} [W m^{-1} K^{-1}]
	Specific heat capacity, C_p	1100 [J kg^{-1} K^{-1}]

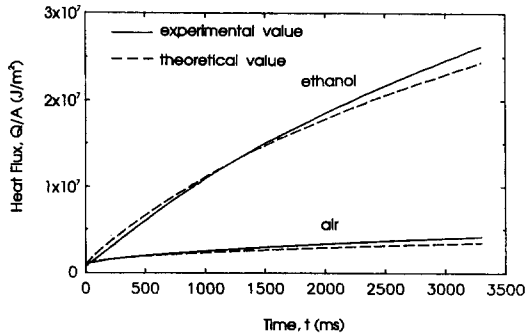

Fig. 4. Calibration of heat probe in ethanol and air.

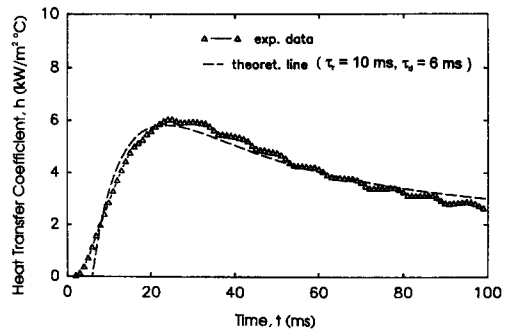

Fig. 5. Comparison of experimental h and predicted h by using probe response time $\tau_r = 10$ ms.

and the heat loss was calculated assuming heat conduction to a semi-infinite medium. The second term, i.e. conduction through the substrate, was calculated by using the thermal properties of expanded polystyrene shown in Table 1. The results of the calculation are shown in Fig. 4, where the total heat dissipated by the probe is plotted as a function of time. From Fig. 4, it can be seen that the theoretical prediction using the physical properties of the substrate and fluid, given in Table 1, are close to the experimentally measured values. These results serve to confirm the thermal properties of the substrate material.

Additionally, the response time of the probe and associated electronic circuitry was determined. The experimental determination of the response time of the probe was found by exposing the probe to air and starting the control circuit to supply a current to the probe and simultaneously measuring the current passing through the probe and the resistance of the probe. At some time, 1–2 s, after starting the experiment the probe was then suddenly immersed in water, while continuing to record the temperature and current supplied to the circuit. From the above description it is apparent that if thermal contact between the probe and water is achieved in a very short time, it may be assumed that a step change occurs in the heat transfer medium surrounding the probe. In order to find the response time (τ_r), the probe and associated control circuit were assumed to be a first order linear system. The input signal to the system was h_{in}, which was the heat transfer coefficient between the probe and contacting medium, the output signal of the system was h_{out}, which was the coefficient calculated from the measured current and resistance. The relation between the input and output signal is expressed as:

$$h_{out}(t) = \frac{1}{\tau_r} \int_{t_0}^{t} h_{in}(\xi \exp[-(t-\xi)/\tau_r])\, d\xi \qquad (3)$$

where τ_r is the characteristic response time of the probe, h_{out} is calculated based on the measured current and resistance, h_{in} is obtained by modeling the heat transfer process between the water and probe as a semi-infinite medium and t is the time after the air was replaced by the water.

The results of a typical experiment are shown in Fig. 5, where h_{out} is plotted as a function of time after the probe is immersed in water. The slight waviness of the experimental signal is an artifact of the electronic driver circuit and control system for the heat transfer probe. The response time τ_r was found by matching the value of h_{out} computed from equation (3) to that measured experimentally. The best fit between the two profiles was obtained for a value of τ_r equal to 10 ms. The response time of this probe and circuit is consistent with the response times from similar probes, e.g. Catipovic [24] found a response time of 20 ms for a thin film platinum probe. From Fig. 5 it can be seen that there is an additional time lag (τ_d) between the experimental results and theoretical predictions. This time shift arises from the assumption of a linear first order system to describe the system's response. However, the actual probe is probably more accurately described by a coupled set of first order systems which gives rise to an effective second or

higher order system. The magnitude of the error that these time lags cause is addressed in the data processing section.

4. EXPERIMENTAL INVESTIGATION

4.1. *Setup*

The experimental setup used in this study is shown schematically in Fig. 1(a). Fluidizing air, supplied by a compressor, was passed through one of three calibrated rotameters to the plenum chamber located below the distributor plate of the fluidized bed. The air then passed upward through the distributor plate. After passing through the bed, the air was vented to the atmosphere. The instrumentation within the bed is shown in Fig. 1(b) and is described in Section 3 above.

4.2. *Experimental conditions*

All the experimental work was carried out at room temperature and atmospheric pressure. The experimental parameters varied in this work were: (1) particle size, (2) the frequency and amplitude of the vibrating bar and (3) the air velocity through the fluidized bed column. These experimental parameters are summarized in Table 2.

The air velocity through the fluidized bed column was set at the critical air velocity u_0 which was defined here as the gas velocity under which no natural particle motion, caused by air flow, was detectable by the heat probe. Since the purpose of this work was to study the effect of relative motion between particles and heat transfer surface on the heat transfer process, without natural particle motion interference, the air velocity should be sufficiently low so that no natural particle motion existed. However, it was found that at very low air flow rates particles in the column were firmly packed, and the vibration bar immersed in the particles would not vibrate due to the large frictional forces caused by these firmly packed particles. By increasing the air flow rate through the bed, to the critical value shown in Table 2, it was found that the vibrating bar could overcome the frictional forces and oscillate freely. In addition, there was no observable bubble formation in the vicinity of the probe either when the probe was stationary or oscillating. Thus by carrying out the experimental program at the critical air velocity the effects of local gas bubbling were eliminated. Since the particle size and critical air velocity are related, there were only three independent experimental parameters: particle size, vibration frequency and amplitude.

Table 2. Summary of experimental conditions

Particle size, d_p [μm]	496,1035
Particle material shape	Glass/spheres
Vibration amplitude, δ_{vib} [μm]	200,500
Vibration frequency, f [Hz]	0, 2, 6, 10
Critical air velocity, u_c [m s^{-1}]	0.158, 0.586

4.3. *Experimental procedure*

Particles (d_p = 496 or 1035 μm) were poured into the fluidized bed column to a static bed height of about 0.2 m. Air from the blower was metered by one of the three flow meters. These flow meters were calibrated against a wet test meter and high accuracy flowmeters. The air flow rate was adjusted to the level corresponding to the critical air velocity for the given particle size.

The vibration amplitude of the vibration device was set to one of the two levels (200 or 500 μm) by adjusting the set screws at each end of the vibration bar. The vibration frequency was set to one of the four levels (0, 2, 6 and 10 Hz) by adjusting a capacitor in the timer circuit.

The heat probe circuit, providing current to the heat probe, was turned on, and simultaneously the current passing through the probe and the resistance of the probe were measured. The data were recorded on an AT Zenith computer through a Keithley 570 data acquisition station.

5. EXPERIMENTAL RESULTS AND DISCUSSIONS

5.1. *Data processing*

Equations for computing heat transfer coefficients were obtained from modeling the heat transfer process around the heat transfer probe, and are documented in detail by Du [23]. The instantaneous and time averaged heat transfer coefficients between fluidized particles and the heat probe were calculated according to the following equations:

$$h = \frac{q_{bed}}{A(T - T_0)} \tag{4}$$

$$\bar{h} = \frac{1}{t}\int_0^t h(\xi)\,d\xi. \tag{5}$$

In addition, equation (6)–(10) were solved simultaneously in order to estimate the instantaneous values of the heat transfer coefficients. For this analysis, the heat transfer to the substrate was modelled as a one-dimensional semi-infinite conduction problem. The accumulation of energy within the tin foil was estimated from a simple transient lumped model, which is justified due to the small thermal capacity of the tin foil element:

$$q_{bed} = p - q_{tin} - q_{sub} \tag{6}$$

$$p = I^2 R \tag{7}$$

$$q_{tin} = (\rho C_p A z)_{tin}\frac{dT}{dt} \tag{8}$$

$$q_{sub} = (\rho C_p A)_{sub} \left[\frac{\alpha_{sub}}{\pi}\right]^{1/2} \int_0^t (t-\xi)^{-1/2} \frac{dT}{d\xi} d\xi \quad (9)$$

$$T = T_0 + \frac{(R-R_0)}{\beta R_0}. \quad (10)$$

The thermal properties of the tin foil and substrate, taken from Weast [25], Alfa Chemicals [26], Karasz *et al.* [27] and Jakob [28], are listed in Table 1. Based on equations (4)–(10), and using the above thermal properties, h and $\bar{h}$ were computed from the measured current (I) and resistance (R) of the probe.

From the above set of equations it is possible to determine the instantaneous heat transfer coefficient, h. However, this is not the true value of h, since the electronics have a non-zero response time. In order to estimate the true value of h, equation (3) must be solved to obtain the kernel, $h_{in}(\xi)$. The deconvolution of equation (3) is quite involved and the details are given elsewhere, Du [23]. The results of this analysis showed that for the vibration frequencies used in this work (10, 6 and 2 Hz), the average error caused by the response time τ_r and time lag τ_d is small (2%, 1% and less than 1%).

5.2. *Packed bed results*

In order to further verify the accuracy of the probe and method of data analysis, a series of experiments were performed using the stationary probe in packed beds of glass particles. Figures 6 and 7 present the results for packed beds with particle sizes of 496 and 1035 μm, respectively. For comparison, the predictions of a modified Mickley and Fairbanks's model, due to Kunii and Levenspiel [1], are included in Figs. 6 and 7. This model assumes that there are two heat transfer resistances in series contained in particles near a heating surface; $1/h_w$, being the resistance of the layer of particles next to the heat transfer surface, and $1/\bar{h}_e$, being the resistance of the particles in the bulk emulsion. An expression for the time averaged overall heat transfer resistance, $1/\bar{h}$, is obtained by summing h_w and $\bar{h}_e$ and is given below in equations (11)–(13):

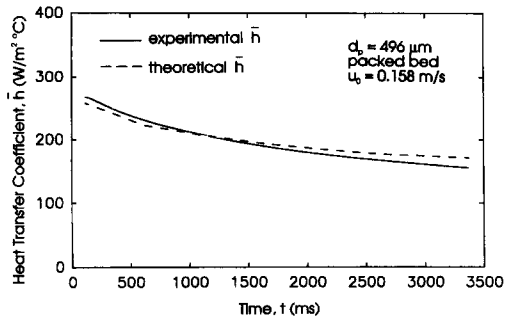

Fig. 6. Comparison of experimental data with the modified Mickley and Fairbanks's model for $d_p = 496$ μm particles.

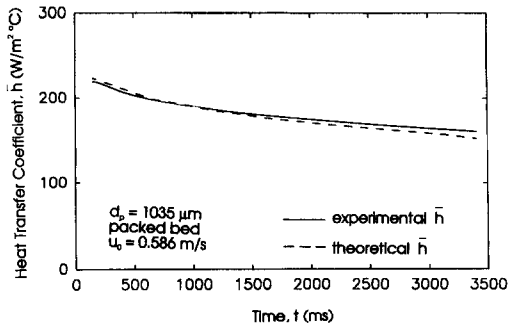

Fig. 7. Comparison of experimental data with the modified Mickley and Fairbanks's model for $d_p = 1035$ μm particles.

$$\frac{1}{\bar{h}} = \frac{1}{h_w} + \frac{1}{\bar{h}_e} \quad (11)$$

where

$$h_w = \frac{2k_{ew}}{d_p} + KC_{p,g}\rho_g u_0 \quad (12)$$

and

$$\bar{h}_e = 2\left[\frac{k_e \rho_s (1-\varepsilon_{mf}) C_{p,s}}{\pi t}\right]^{1/2}. \quad (13)$$

The parameters used in this model were obtained by fitting previous experimental data for packed bed heat transfer and expressions are given in Kunii and Levenspiel [1].

The experimental results for packed beds of 496 and 1035 μm particles are given in Figs. 6 and 7, respectively. From these figures it can be seen that the experimentally determined values of the time averaged heat transfer coefficients for both sizes of particles are in very good agreement with the predictions of the modified Mickley and Fairbank's model. The average error for both particle sizes is $\pm 5\%$.

5.3. *Vibrating bed experiments*

In Fig. 8, the heat transfer coefficients for the smaller particles, $d_p = 496$ μm, using an amplitude of vibration (δ_{vib}) of 500 μm and frequencies of $f = 2$, 6 and 10 Hz are given. Figure 9 presents the coefficients for the larger particles, $d_p = 1035$ μm, using an amplitude of vibration (δ_{vib}) of 500 μm and frequencies $f = 2$, 6 and 10 Hz. Figure 10 presents the results for the larger particles, $d_p = 1035$ μm, under the same conditions as given above except with an amplitude of vibration (δ_{vib}) of 200 μm. Comparing the instantaneous heat transfer coefficients for $f = 2$, 6 or 10 Hz with those for a packed bed ($f = 0$ Hz), one can see that the periodic motion between the particles and heat transfer surface causes periodic fluctuations in the heat transfer coefficients. This conclusion is consistent with the prediction of the model due to Du and Turton [9].

For a given size of particle, a larger vibration amplitude produces a larger variation in instantaneous heat transfer coefficient, as indicated in Figs. 9 and 10. It

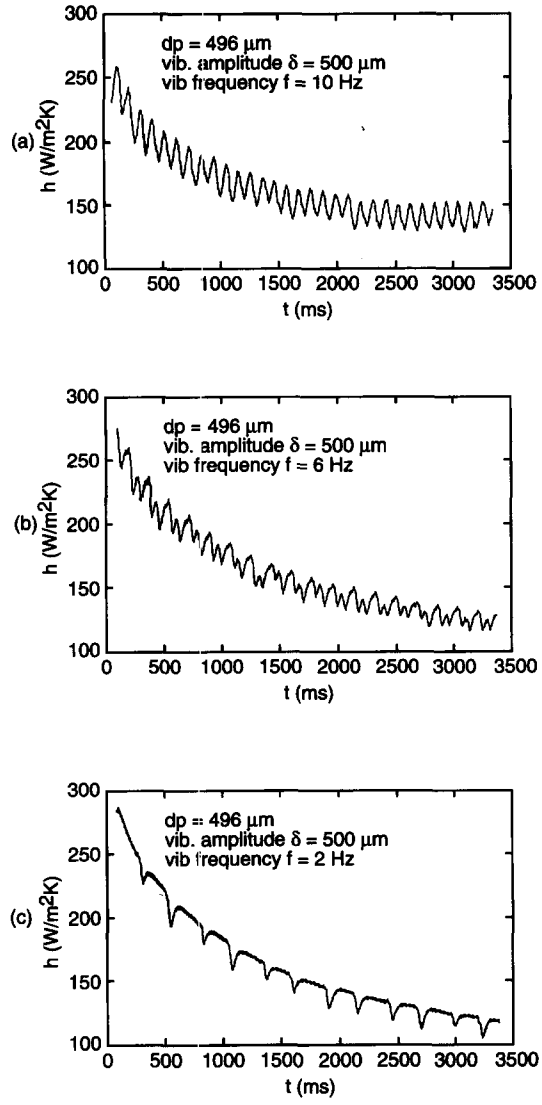

Fig. 8. Heat transfer coefficients for $d_p = 496$ μm particles at $\delta_{vib} = 500$ μm and $f = 2$, 6 and 10 Hz.

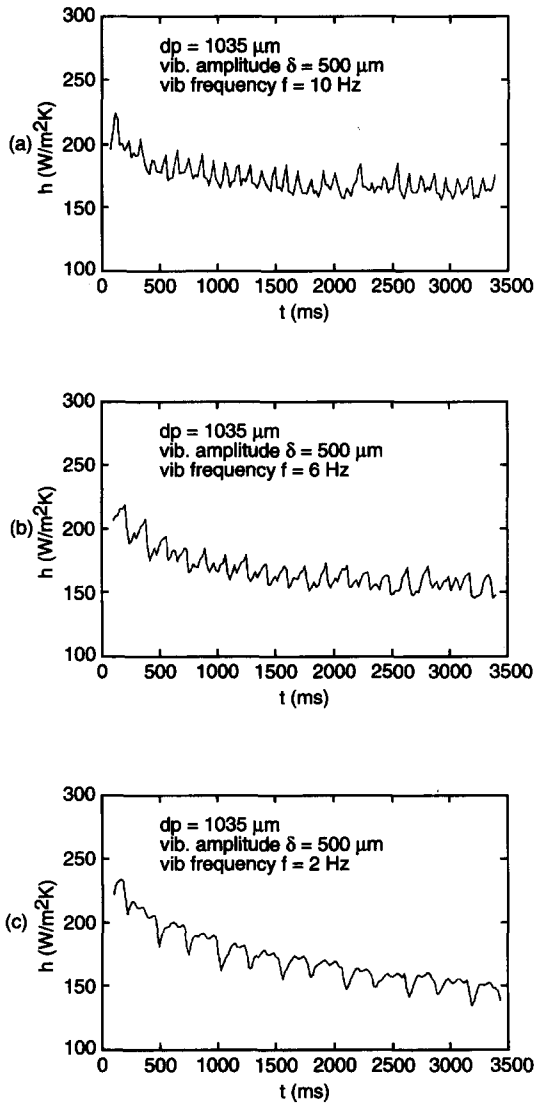

Fig. 9. Heat transfer coefficients for $d_p = 1035$ μm particles at $\delta_{vib} = 500$ μm and $f = 2$, 6 and 10 Hz.

is believed that the larger vibration amplitude causes an increase in the voidage near the heat transfer surface thus giving rise to larger variations in the heat transfer coefficient.

Figures 8 and 9 indicate that heat transfer coefficients fluctuate at approximately the same frequency as the vibration frequency for $f = 10$ and 6 Hz, but at about twice the vibration frequencies for $f = 2$ Hz. This phenomenon is believed to be caused by the motion of the bar and particles near the vibrating surface. As confirmed by visual observation, Du [23], the motion of the vibrating surface creates a variation in voidage near the vibrating surface.

The motion of the bar follows a square wave. Therefore, the movement of the heat transfer probe consists of a half cycle where the heat transfer surface moves forward through the particle bed and then pauses, followed by a second half cycle where the surface moves away from the bed and then pauses. At low applied frequencies it is believed that the particles can follow exactly the movement of the probe and hence a heat transfer event occurs at every half cycle during the vibration. This heat transfer event results always in a reduction in the observed heat transfer coefficient. During the half cycle where the surface moves away from the bed a small air gap or region of high voidage would be briefly formed at the surface and this would lead to a reduction in h. For the other half cycle, where the surface moves forward through the bed of particles, it might be expected that the value of h would increase or remain constant rather than decrease, as was observed. It is possible that at the end of this half cycle the particles have sufficient inertia that they continue to move away from the now stationary surface, again forming a region of high voidage at the surface and causing the heat transfer coefficient to decrease. At higher frequencies, the inertia of the particles prevents them following the applied vibration

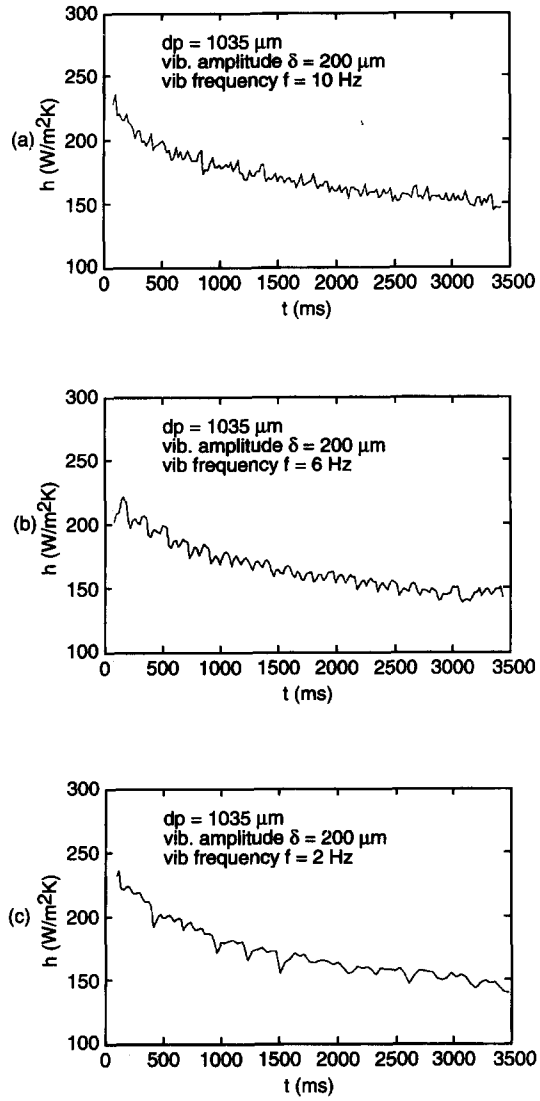

Fig. 10. Heat transfer coefficients for $d_p = 1035$ μm particles at $\delta_{vib} = 200$ μm and $f = 2$, 6 and 10 Hz.

frequency and hence only a single heat transfer event occurs every cycle. Further work needs to be done in order to verify this phenomenon.

Finally, it is interesting to note the time averaged heat transfer coefficients for the packed bed and vibrating heat transfer surface experiments, for a given particle size, were very similar. However, higher vibration frequencies appear to promote higher heat transfer coefficients at later times, for both particle sizes studied.

6. CONCLUSIONS

The heat transfer coefficients between a heat transfer surface and a packed bed of particles in air at atmospheric pressure were measured. The time averaged heat transfer coefficient was estimated using a modified Mickley and Fairbanks's model, given by Kunii and Levenspiel [1], and a comparison with the experimental data showed good agreement.

The heat transfer coefficients between fluidized particles and a vibrating heat transfer surface were measured. The main finding obtained from these data was that the cycling motion between the particles and the surface produced a cycling variation in the heat transfer process. The vibration amplitude (δ_{vib}) was the main factor affecting the fluctuation amplitude of the instantaneous heat transfer coefficient. Variations in heat transfer coefficients of up to 30 W m^{-2} K^{-1} were observed. It was postulated that the fluctuations of the instantaneous heat transfer coefficient were caused by the voidage change of the particles near the vibrating heat transfer surface. The frequency of the fluctuating heat transfer component was the same as the frequency of the motion of the surface for the data taken at 10 and 6 Hz. However, the heat transfer fluctuations were approximately twice the applied frequency for the data taken at 2 Hz.

Acknowledgements—The authors would like to acknowledge that funding for this work was provided under National Science Foundation grant CBT-865754

REFERENCES

1. D. Kunii and O. Levenspiel, *Fluidization Engineering* (2nd Edn), p. 90. Butterworth-Heinemann, Boston, MA (1991).
2. J. R. Grace, Contacting modes and behavior classification of gas–solid and other two-phase suspension, *Can. J. Ch. E.* **64**, 353–363 (1986).
3. R. D. Toomey and H. F. Johnstone, Gaseous fluidization of solid particles, *Chem. Engng Progr.* **48**(5), 220–226 (1952).
4. K. Hilligardt and J. Werther, Local bubble gas hold-up and expansion of gas–solid fluidized beds, *German Chem. Engng* **9**, 215–221 (1986).
5. P. N. Rowe and B. A. Partridge, An X-ray study of bubbles in fluidised beds, *Trans. Instn Chem. Engng* **43**, T157–Y175 (1975).
6. L. Massimilla and J. W. Westwater, Photographic study of solid–gas fluidization, *A.I.Ch.E.Jl* **6**, 134–138 (1960).
7. N. A. Decker, Heat transfer to horizontal tubes in large particle gas fluidized beds, Ph. D. Thesis, Massachusetts Institute of Technology, Cambridge, MA (1983).
8. J. F. Davidson and D. Harrison, *Fluidised Particles*, p. 70. Cambridge University Press, Cambridge, U.K. (1963).
9. C. Du and R. Turton, A theoretical study of the limiting heat transfer coefficient in fluidized beds, *Chem. Engng Commun.* **121**, 99–123 (1993).
10. H. S. Mickley and D. F. Fairbanks, Mechanism of heat transfer to fluidized beds. *A.I.Ch.E.Jl* **1**, 374–384 (1955).
11. A. P. Baskakov, Transfer of heat from an isothermal surface to a continuous flow of dispersed medium, *Heat Transfer—Sov. Res.*, **4**(6), 103–107 (1969).
12. J. Kubie and J. Broughton, A model of heat transfer in gas fluidized beds, *Int. J. Heat Mass Transfer*, **18**, 289–299 (1975).
13. R. Chandran and J. C. Chen, A heat transfer model for tubes immersed in gas fluidized beds. *A.I.Ch.E.Jl* **31**, 244–252 (1985).

14. R. Ernst, The mechanism of heat transfer to heat exchangers in fluidized beds, *Chem.-Ing. Techn.* **31,** 166–173 (1959).
15. R. Ernst, Heat transfer to heat exchangers in moving beds, *Chem.-Ing. Techn.* **32,** 17–22 (1960).
16. J. S. M. Botterill and J. R. Williams, The mechanism of heat transfer to gas fluidized beds, *Trans. Instn Chem. Engrs* **41,** 217–230 (1963).
17. J. S. M. Botterill and L. N. Hampshire, The gap between surface and particles in relative motion, *Chem. Engng Sci.* **42**(4), 400–402 (1968).
18. E. U. Schlünder, Heat transfer to moving spherical particles at short contact times, *Int. Chem. Engr.* **20**(4), 550–554 (1980).
19. E. Muchowski, Heat transfer from the bottoms of vibrated vessels to packings of spheres at atmospheric pressure and under vacuum, *Int. Chem. Engr* **20**(4), 564–576 (1980).
20. J. Wunschmann and E. U. Schlünder, Heat transfer from a heated surface to spherical packings, *Int. Chem. Engr* **20**(4), 555–563 (1980).
21. N. A. Decker and L. R. Glicksman, Conduction heat transfer at the surface of bodies immersed in gas fluidized beds of spherical particles, *A.I.Ch.E. Symp. Ser.* **77**(208), 341–349 (1981).
22. G. Gloski, L. R. Glicksman and N. Decker, Thermal resistance at a surface in contact with fluidized bed particles, *Int. J. Heat Mass Transfer* **27**(4), 599–610 (1984).
23. C. Du, A study of limiting heat transfer coefficients in a fluidized bed, Ph.D. Dissertation, West Virginia University, Morgantown, WV (1992).
24. N. M. Catipovic, Heat transfer to horizontal tubes in fluidized beds : experiment and theory Ph.D. Thesis, Oregon State University, Corvallis, OR (1979).
25. R. C. Weast (Editor), *CRC Handbook of Chemistry and Physics* (66th Edn). CRC Press, Boca Raton, FL (1986).
26. Alfa Chemicals, Alfa Catalog (Research Chemicals and Accessories), Johnson Matthey, Alfa Products, Wardhill, MA (1992).
27. F. E. Karasz, H. E. Bair and J. M. O'Reilly, Thermal properties of atactic and isotactic polystyrene, *J. Phys. Chem.* **69**(8), 2657–2667 (1956).
28. M. Jakob, *Heat Transfer* (1st Edn), Vol. 1, p. 107. Wiley, New York (1949).